

GA-A25663

**REDUCTION OF ISOLATED DEFECTS ON  
Ge DOPED CH CAPSULES TO BELOW  
IGNITION SPECIFICATIONS**

by

**K.C. CHEN, Y.T. LEE, H. HUANG, J.B. GIBSON, A. NIKROO,  
M.A. JOHNSON, and E. MAPOLES**

**JANUARY 2007**



## **DISCLAIMER**

This report was prepared as an account of work sponsored by an agency of the United States Government. Neither the United States Government nor any agency thereof, nor any of their employees, makes any warranty, express or implied, or assumes any legal liability or responsibility for the accuracy, completeness, or usefulness of any information, apparatus, product, or process disclosed, or represents that its use would not infringe privately owned rights. Reference herein to any specific commercial product, process, or service by trade name, trademark, manufacturer, or otherwise, does not necessarily constitute or imply its endorsement, recommendation, or favoring by the United States Government or any agency thereof. The views and opinions of authors expressed herein do not necessarily state or reflect those of the United States Government or any agency thereof.

# REDUCTION OF ISOLATED DEFECTS ON Ge DOPED CH CAPSULES TO BELOW IGNITION SPECIFICATIONS

by

K.C. CHEN, Y.T. LEE, H. HUANG, J.B. GIBSON, A. NIKROO,  
M.A. JOHNSON,\* and E. MAPOLES\*

This is a preprint of a paper presented at the 17th Target  
Fabrication Specialist Meeting, San Diego, California on  
October 1-5, 2006 and to be published in *Fusion Science and  
Technology*.

\*Lawrence Livermore National Laboratory, Livermore, California.

Work supported by  
the U.S. Department of Energy  
under DE-AC03-01SF22260 and W-7405-ENG-48

GENERAL ATOMICS PROJECT 30272  
JANUARY 2007



## REDUCTION OF ISOLATED DEFECTS ON Ge DOPED CH CAPSULES TO BELOW IGNITION SPECIFICATIONS

K.C. Chen, Y.T. Lee, H. Huang, J.B. Gibson, A. Nikroo, M.A. Johnson,<sup>1</sup> and E. Mapoles<sup>1</sup>

General Atomics, P.O. Box 85608, San Diego, California 92186-5608

<sup>1</sup>Lawrence Livermore National Laboratory, Livermore, California 94550  
chenkc@fusion.gat.com

*The NIF Ge-doped CH capsule should be free of isolated defects on the outer surface. The allowed number and dimensions of large isolated defects over the entire capsule surface is given by the isolated feature specification.*

*To date NIF-thickness (146  $\mu\text{m}$ ) capsules are plagued by a few isolated large domes on the outer surfaces that otherwise meet the atomic force microscope (AFM) spheremap modal power spectra specification. The large domes on the capsule surfaces were mostly caused by particulate contamination from the wear of an agitation tapping solenoid inside the coater. By eliminating the solenoid and using an alternate rotation agitation, most thick-walled capsules become free of large isolated defects and meet the AFM spheremap modal power spectra standard.*

*The number and size of the isolated defects on the outer surface were characterized with a high resolution phase-shifting diffractive spherical interferometer and checked against the NIF isolated defect specification. The results show the isolated defects on the rolled capsule are below the isolated defect specification. The growth modeling of the remaining nanometer-height domes on the capsules indicates most of these small domes come from the mandrel surface.*

*The rolled capsules meet the layer thickness, doping levels and wall thickness specifications and have good wall uniformity of  $\pm 0.1\text{--}0.2 \mu\text{m}$ .*

### I. INTRODUCTION

Germanium-doped CH capsule is one of the ablator designs for the National Ignition Facility (NIF). The surface finish of Ge-doped CH capsule is governed by the AFM modal power spectra requiring surface roughness on the order of 10 nm rms or less. The AFM power spectra are a good indication of surface finish when the surface is uniformly rough. However, when the isolated features

becomes fewer and scattered, the chance of encountering isolated defects with AFM spheremap lessens.

The capsule surface needs to be free of large isolated defects to ensure that the final perturbation on the fuel is small at peak velocity. The permissible size and number of large isolated surface defects over the entire capsule surface is given by the NIF isolated feature specification, as shown in Fig. 1 that defines the number and the allowed dimensions of the surface features binned into three frequency regions.<sup>1</sup>

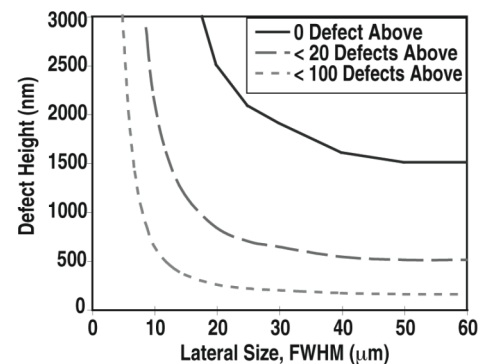


Figure 1. The NIF isolated feature specification defines the allowed number and dimensions of isolated defect features on the outer surface of the capsule.

To date, NIF-thickness (146  $\mu\text{m}$ ) CH capsules, otherwise meeting the AFM modal power spectra standard, have been plagued by a few large isolated defects (mostly domes) on the outer surface. There have been numerous publications on the cause of these isolated domes. Many dome sources have been identified, including the effect of mandrel surface chemistry, the existence of microscopic defects on mandrel, abrasion damage from mechanical agitation, deposition parameters and transient state gas phase particulate nucleation.<sup>2-7</sup> Methods of in-process gas etching and post-coating polishing to eliminate isolated domes are being tried.<sup>8,9</sup>

*K.C. Chen, et al.*

According to the isotropic growth model, domes with large lateral sizes originate at the beginning of the coating process.<sup>5</sup> We have observed some of these large domes to have visible dark-spot origins deep within the wall. The visible origins indicate possible particulate contamination. In this study, we focused on the investigation and removal of particulate sources from inside the coater chamber because, if they exist, they have a high probability of contaminating the coating.

## II. EXPERIMENTS

The investigation of particulate contamination inside the chamber examined the process steps from loading mandrels into chamber to removing the finished capsules from the chamber. Any movable items between these two events are considered to be potential contamination sources. Figure 2 shows the movable items identified in the coater: (1) plasma tube changes; (2) opening and assembling the upper and lower coater chambers for a plasma tube change or performing a coating rate check; (3) screw attachment for pan holding and (4) impacts and motions of tapping solenoid to agitate the capsules. Only (4) has prolonged movements during the coating run while others are intermittently moved. Since the above listed items are all moved at least once in a lengthy coating run, they might have all contributed to the particulate contamination to some degree. We resolved to enhance or inhibit the effects of one or several movable items in order to understand their contributions on particulate contamination.

Freshly-cleaved mica pieces (2.5 cm × 2.5 cm) with smooth pristine surfaces were used as mandrel surrogates for particulate contamination studies. The use of mica eliminates the uncertainty of whether the dome source is from the mandrel. After each coating experiment, the central 1 cm × 1 cm area of mica was scanned for large domes with a WYKO interferometer. The central 1 cm<sup>2</sup> area is of interest because it is where shells are usually located in the pan. Furthermore, the area is also comparable to the total surface area of 9 shells used for a typical NIF capsule run. The diameter and height of the domes were measured and plotted against NIF isolated defect specification. The total number of domes above the lowest curve of Fig. 1 was counted altogether as “critical” domes.

A rotation setup was built specifically to coat NIF capsules. The setup eliminates the tapping agitation solenoid. In addition, a drop-in pan holder design eliminated the need for screw attachment. The pan has a 10° tilt angle and rotates at 12 rpm during coating. The surface finish of the rolled graded germanium CH

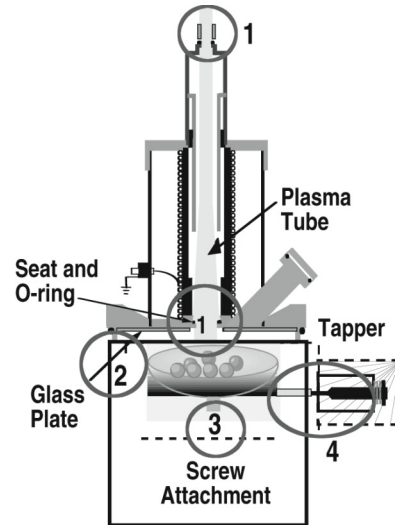


Figure 2. The locations of the movable parts inside the coating chamber. The movable parts are considered possible particulate sources, including (1) contact regions from plasma tube change; (2) contact from the assembling of the upper and lower chambers after plasma tube changes or thickness checks; (3) pan screw attachment and (4) tapping solenoid for agitation.

capsules was characterized by AFM spheremap.<sup>10</sup> The layer thicknesses, germanium doping levels, wall uniformity were measured from quantitative contact radiographs, as described previously.<sup>10,11</sup>

The isolated defects on the capsule surface were measured with a spherical phase-shifting diffractive interferometer (PSDI) developed at Lawrence Livermore National Laboratories. The details of the principle and construction of the PSDI have been described elsewhere.<sup>12,13</sup> In brief, the phase shifts and intensities from the interferometer images were propagated to obtain the height and lateral size of the defects on the capsule surface. A threshold of 50 nm was chosen so that only dome height larger than 50 nm is counted. This threshold is chosen since domes below 50 nm height are below the critical regions of NIF isolated feature specification, as illustrated in Fig. 1. The software automatically searched for regions that exceeded the 50 nm threshold, located the highest points within the regions and then reported the full-width at the half-maximum (FWHM) of every identified region.

Each PSDI image covers a 500 μm diameter area. Eighteen images are needed to cover an equator band, with one duplicate image to confirm the repeatability. Sixty-nine images are required to cover a hemisphere of a 2 mm capsule and take approximately 1 h. The

hemisphere measurement covers about 60% of the capsule surface, with five duplicate images to verify the repeatability. Adjacent images are overlapped so there is no gap between images. The pixel size of the image is 0.68-0.84  $\mu\text{m}$ , thus the lateral resolution of PSDI is better than 1  $\mu\text{m}$ . The peak to valley height accuracy is  $\sim 5$  nm.

Several capsules were selected from three coating runs for isolated feature characterization. The capsules can be characterized with PSDI only after the capsule heat treatment in a nitrogen atmosphere to remove the mandrel, rendering them dark-colored. The as-coated capsules are too transparent and signals from the opposite wall caused unwanted interference. Equatorial bands (20% surface coverage) of several capsules were first measured and then hemisphere measurements (60% surface coverage) were done as automatic precision detector positioning device became available.

### III. RESULTS

#### III.A. Identification of Particulate Contamination Source from Mica Experiments

Mica surrogate experiments were designed to identify and to eliminate the possible particulate sources. Each experiment has two plasma tube changes and each change was followed by a 20  $\mu\text{m}$  CH coating in order to grow the particulates into visible domes. The results are shown in Fig. 3.

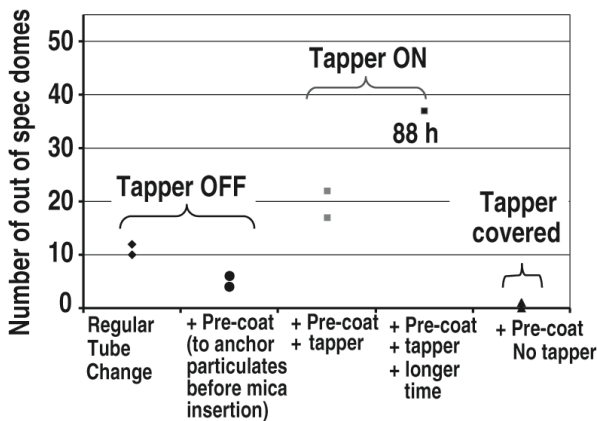


Figure 3. The particulate contamination experiments used mica pieces as mandrel surrogates. The dome count increase with the use of tapping solenoid. Covering the tapper reduces the dome count, indicating that the presence of tapper in the chamber, even without movement, is still a contamination source. Except for 88 h run, each contamination experiment is repeated 2–3 times.

The first and the second experiments were done with the tapping agitation solenoid turned off. The first

experiment is a baseline run that mimics two plasma tube changes but pays little attention to the tube insertion practice. The data seems to show several particulates from tube insertion and or assembling the upper and lower chambers. The second experiment was done to reduce the particulate contamination from plasma tubes change by carefully inserting a freshly-cleaned plasma tube and then carefully dusting off the end of the plasma tube with compressed air after the tube went through the glass plate. A 2 h coating run was done after the plasma tube changes before the mica piece was introduced. The 2 h coating practice is to anchor any imperceptible particulates from the plasma tube changes so the contribution from chamber assembling at the mica insertion can be seen. The data showed reduction of dome count (Fig.3).

The third and fourth coating runs tested the effect of when the agitation tapping solenoid was turned on. Otherwise, the coating parameters were identical to the second experiment. The dome count roughly doubled as compared to the base line result. The dome count also increased in the fourth run, during which the coating time was nearly doubled and hence doubled the number of the tapping plunger movements. These two experiments clearly revealed the tapping solenoid was a particulate contamination source. During the fifth run the contribution of tapping solenoid was inhibited by sealing it from the coating chamber with aluminum foil. Only one or no dome was found on micas in repeated runs. Comparing the results of the second and fifth experiments, we concluded that the tapping solenoid, even without being energized, contributed some particulates into the coating chamber during the vacuum pump down.

After taking apart the tapping solenoid, particulates from the wear of the barrel liner were found rubbing against the plunger (Fig. 4). The particulates on the plunger were examined with scanning electron microscope. The size of the particulates was determined by dust them off onto mica and then characterized with WYKO interferometer. The particulate size ranges from tens of nanometer to tens of micrometer. The particulate is plastic in nature. From radiograph images, we did not see evidence of metallic particulates, so there is no contamination from the pan screw.

#### III.B. Reduction of Isolated Defects on Rolled Germanium-Doped Capsules

Since the tapper solenoid is the major particulate contamination source, the tapper solenoid was removed from the coater and a rotating setup was built to agitate the capsules. The optical photograph of the rolled capsules clearly shows the reduction of large domes, as compared to the tap-agitated capsule shown in Fig. 5. The

AFM ( $3 \times 3$ ) traces show no domes higher than 200 nm and power spectra are below the surface modal power spectrum standard [Fig. 6(a) and 6(b)]. The high modes ( $>11$ ) are in the range of 3–6 nm.

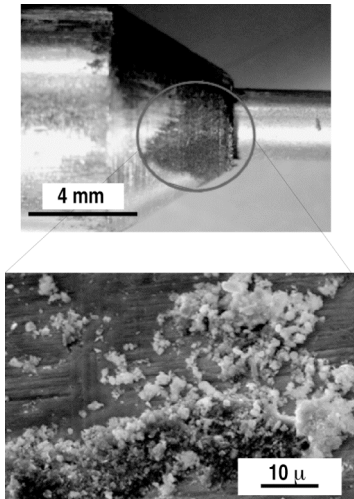


Figure 4. The particulates collect on plunger from the wear of the barrel of the solenoid. The size of particulates on the plunger surface ranges from nm to  $\mu\text{m}$ .

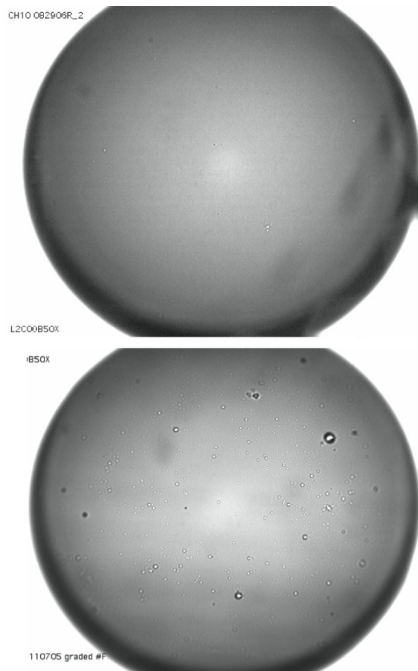


Figure 5. The optical images of NIF capsules coated using rotation agitation (top) and tapping solenoid agitation (bottom). The capsule coated without the presence of the tapping solenoid shows a great reduction of large domes.

The complete AFM spheremap was insufficient for isolated defect characterization because it is a line-tracing

REDUCTION OF ISOLATED DEFECTS ON GE DOPED CH CAPSULES TO BELOW IGNITION SPECIFICATIONS

technique so there is a finite distance between adjacent AFM traces. Domes with a lateral size smaller than the distance between adjacent traces may not be counted. Also, traces do not always cross the defect apexes, so the defect height and lateral size are likely to be understated. Complete spheremap might overestimate the number of large domes since several traces will pass over the same large dome, unless adjacent traces are checked for the multiple counting. On the other hand, PSDI is an aerial mapping method with no gap between adjacent pixels and no gap when overlapped images are taken. It has lateral resolution better than  $1 \mu\text{m}$  and height resolution of  $\sim 5 \text{ nm}$ . Therefore, PSDI was used to characterize the isolated defects.

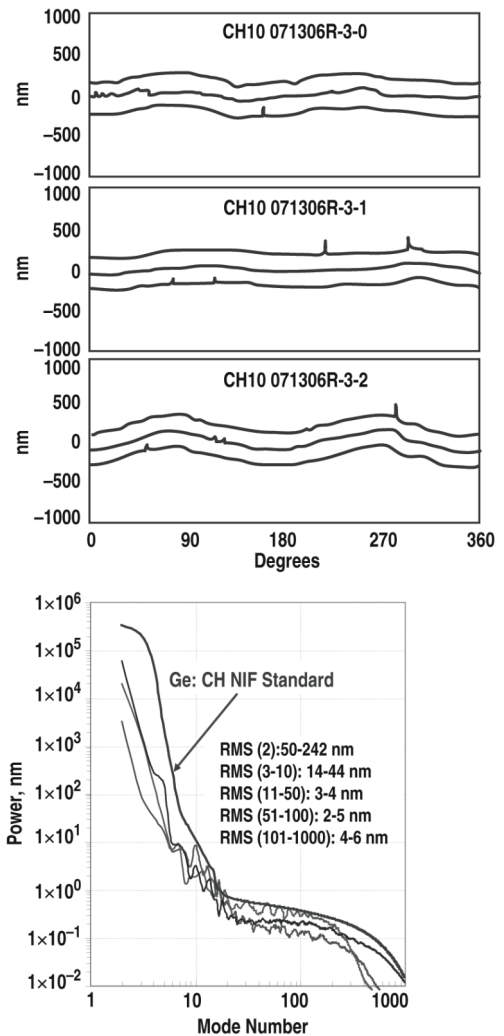


Figure 6. AFM spheremap traces of a  $146 \mu\text{m}$  Ge:CH capsule and three average AFM power spectra from three rolled capsules.

A typical propagated PSDI image is shown in Fig. 7. A threshold of 50 nm was chosen so that only domes with a height greater than 50 nm are shown. As stated before,

domes with less than 50 nm height are inconsequential to the NIF isolated feature specification since they are below the three critical frequency regions in the NIF isolated defect specification in Fig. 1.

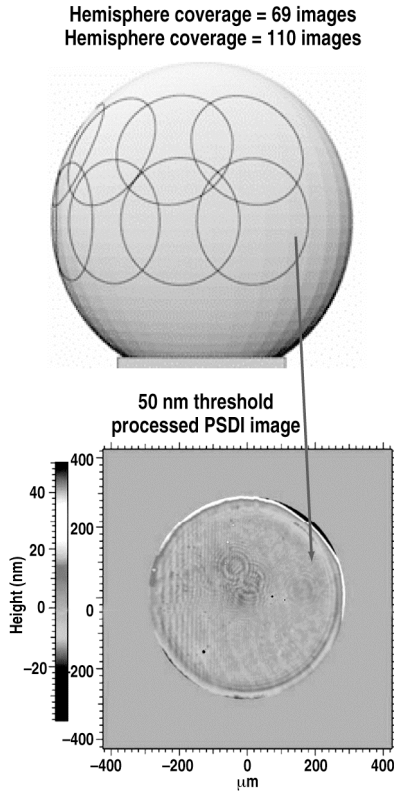


Figure 7. The hemisphere surface coverage requires 69 overlapped PSDI images for a 2 mm size capsule. The image to the right is propagated from the phase and intensity information and shows four domes above 50 nm threshold.

Three capsules characterized using PSDI with equatorial bands and two characterized with hemisphere coverage meet the isolated defect specification. The data of three capsules with one equatorial band and two capsules with hemisphere-coverage are shown in Fig. 8 (a) and (b). If domes are in the three critical regions, we then check if the same domes are multiple-counted from the overlapped areas in adjacent images (Fig 7 top graph for the overlapped areas in adjacent PSDI circular images). No effort was made to check whether the same dome appears in two or more PSDI adjacent images if the domes height is below the lowest frequency regions in NIF isolated feature plot. From the plot, we also notice there are divots of shallow depressions. We also calculated the power spectra (good for modes > 100) from PSDI images. The calculations show that most images have power spectra below the NIF modal power spectra specification.

From Fig. 8, we found that the small domes show a distinct ratio of height and lateral size in a manner previously reported by Letts, et al.<sup>5</sup> According to an isotropic growth model in reference 5, when the dome height ( $h$ ) is either much smaller than the coating thickness ( $t$ ) or dome diameter ( $2W$ ) (i.e.  $h \ll t$  or  $h \ll 2W$ ), the dome diameter ( $2W$ ) grow as a function of the coating thickness ( $t$ ) from a given dome starting point to the outer surface of the capsule:

$$W^2 = 2ht \quad (1)$$

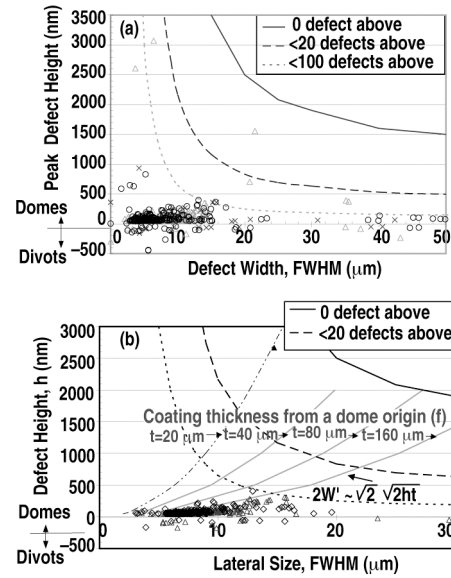


Figure 8. (a) Isolated domes and divots plot of three NIF-thickness capsules characterized with a PSDI equatorial band (18 images). The capsules are below NIF isolated defect specification. The capsule represented with open triangles is made from a 1.7 mm o.d. mandrel batch. The other two capsules are prepared from a mandrel batch with 2 mm o.d. (b) Isolated defect data of two NIF-thickness 2 mm capsules with hemisphere coverages (each has 69 images and covers 60% of the capsule outer surface) shows capsules have no dome are in the upper most critical region (0 dome above) of the NIF isolated defect meet specifications. The four parabolic curves in the plot, with coating thickness next to them, are the calculated lateral size of the domes when coating thickness (distance between a dome origin and outer surface of the shell) reaches the values shown beside the curves.

We wish to apply the isotropic growth model to the PSDI dome diameter data to understand the source of the dome defects. However, the PSDI technique reports the FWHM dome diameter and not the diameter at the base of the dome so direct application of the model is not appropriate. One can make a correction to the dome diameter from the isotropic growth model to fit the PSDI

K.C. Chen, et al.

data if one realizes that, given the assumptions of  $h \ll t$  or  $h \ll W$ , the ratio of the FWHM dome diameter and the diameter at the base of the dome is

$$\sqrt{2}/2 \quad (2)$$

Substituting this correction factor into the equation from the isotropic growth model, with some algebraic manipulation, gives a parabolic function that directly results in FWHM dome diameters:

$$2W' = \sqrt{2}\sqrt{2ht} \quad (3)$$

where  $h$  is the dome height and  $t$  is the coating thickness as before, but  $2W'$  is the FWHM dome diameter for direct comparison with the PSDI data.

We calculated the growth of the lateral size of the domes as a function coating thickness for a series of dome heights using this model. The four calculated parabolic curves, shown in Fig. 8 for 20, 40, 80 and 160  $\mu\text{m}$  coating thicknesses, clearly show a parabolic growth curve left of the data cluster at 160  $\mu\text{m}$  coating thickness. This indicates a growth of the lateral sizes of a group of small domes originates from a depth of 160  $\mu\text{m}$  – the thickness before pyrolysis. Therefore, these nm-height domes are from the mandrel surface. From the graph, we see most of the small domes are to the right of the growth front, which seems to indicate the growth of the lateral size is slightly faster than the prediction of the model. However, it should be pointed out that there are still few domes that originated within the GDP wall. A clear example is a dome (shown in  $\blacktriangle$ ) in the “20 defects above” frequency region in Fig. 8(b). The dome is calculated to start from 20  $\mu\text{m}$  below the outer surface.

### III.C. Characterization of Germanium Doping Levels and Layer Thicknesses

The fabrication of Ge-doped CH capsules to meet doping levels and layer thicknesses has been previously reported.<sup>10</sup> We performed additional coating runs using 1.7 and 2 mm size mandrel batches to determine the reproducibility of the layer thicknesses and doping levels.

Germanium doping levels of  $0.4 \pm 0.1$  at. % and  $0.8 \pm 0.1$  at. % have been achieved, which is within the allowed deviation of the NIF specification. The layer thicknesses and the total thickness are also within the dimension specification. The results of the three 5-shell batches are tabulated against NIF specifications in Table I.

These rolled capsules have the benefit of less wall thickness variation in the capsule than tapped capsules.

The wall thickness variation of  $\pm 0.1$ – $0.2$   $\mu\text{m}$  (standard deviation) in a capsule was achieved, as determined by the unwrapping contact radiographs of the capsule circumferences. Thus, the capsules are able to meet all the major NIF specifications.

Table I. The Layer Thickness, Total Wall Thickness and Doping Levels of Three Different Rolled Capsule Batches

Layers	NIF Specification	Batch 1	Batch 2	Batch 3
4th L	$84 \pm$	$86.6 \pm 0.9$	$86.0 \pm 0.4$	$85.1 \pm 2.1$
3rd L	$10 \pm 2.5$	$10.9 \pm 0.2$	$10.7 \pm 0.5$	$10.6 \pm 0.6$
2nd L	$42 \pm 3$	$41.5 \pm 0.3$	$42.2 \pm 0.4$	$41.7 \pm 0.4$
1st L	$10 \pm 1.5$	$9.7 \pm 0.1$	$9.9 \pm 0.5$	$10.3 \pm 0.6$
Wall	$146 \pm 3$	$146.5 \pm 1.2$	$147.5 \pm 1.6$	$146.5 \pm 0.7$
Ge at. %				
3rd L	$0.4 \pm 0.1$	$0.46 \pm 0.05$	$0.46 \pm 0.05$	$0.48 \pm 0.05$
2nd L	$0.8 \pm 0.1$	$0.73 \pm 0.07$	$0.73 \pm 0.07$	$0.76 \pm 0.08$

## IV. SUMMARY

Most of the large domes on the capsule surfaces were originated from particulate contamination from the wear of tapping solenoid inside the coater. When the tapping solenoid was removed and a new rotation agitation setup was built, the NIF-thickness capsules (146  $\mu\text{m}$ ) met the AFM spheremap power spectra standard.

Several batches of Ge-doped CH capsules were made to meet the NIF composition and layer thickness specifications with rolling agitation. The number and size of the isolated defects on the outer surface of these rolled capsules were characterized using a high-resolution spherical phase-shifting diffractive interferometer. The measurements show the number and size of the domes and divots meet the NIF isolated defect specification. The growth modeling of the remaining nanometer-height domes indicates that most of these small domes come from the mandrel surface. These layer thicknesses, Ge-doping levels, and total wall thickness of these capsules are also within NIF specifications.

## ACKNOWLEDGMENT

Work supported by U.S. Department of Energy under Contracts DE-AC03-01SF22260 and W-7405-ENG-48.

## REFERENCES

1. S. W. HAAN, T. DITTRICH, G. STROBEL, S. HATCHETT, D. HINKEL, M. MARINAK, D. MUNRO, O. JOHNES, S. POLLAINÉ, and L. SUTER, “Update on Ignition Target Fabrication Specifications,” *Fusion Sci. Technol.* **41**, 164 (2002).

2. A. NIKROO, J. BOUSQUET, R. COOK, B. W. MAQUILLAN, R. R. PAGUIO, and M. TAKAGI, "Progress in 2 mm Glow Discharge Polymer Mandrel Development for NIF," *Fusion Sci. Technol.* **45**, 165 (1994).
3. A. NIKROO and D. M. WOODHOUSE, "Bounce Coating Induced Domes on Glow Discharge Polymer Coated Shells," *Fusion Sci. Technol.* **35**, 202 (1999).
4. M. THEOBALD, B. DUMAY, C. CHICANNE, J. BAMOUIN, O. LEGAIE, and P. BACLET, "Roughness Optimization at High Modes for GDP CH<sub>x</sub> Microshells," *Fusion Sci. Technol.* **45**, 176, (2004).
5. S. A. LETTS, D. W. MYERS, and L. A. WITT, "Ultrasoother Plasma Polymerized Coatings for Laser Fusion Targets," *J. Vac. Sci. Technol.* **19**, 739 (1981).
6. S. J. CHOI, P. L. G. VENTZEK, R. J. HOEKTRA, and M. J. KUSHNER, "Spatial Distributions of Dust Particles in Plasma Generated by Capacitively Coupled Radiofrequency Discharge," *Plasma Sources Sci. Technol.* **3**, 418 (1994).
7. A. GARSCADDEN, B. N. GANGULY, P. D. HAALAND and J. WILLIAMS, "Overview of Growth and Behavior of Cluster and Particles in Plasma," *Plasma Sci. Technol.* **3**, 239 (1994).
8. M. THEOBALD, C. CHICANNE, J. BARNOUIN, E. PECHE and P. BACLET, "Gas Etching to Obtain Germanium Doped CH<sub>x</sub> Microshells Compatible with the Laser Megajoule Target Specifications," *Fusion Sci. Technol.* **49**, 757 (2006).
9. D. G. CZECHOWICZ, D. A. STEINMAN, C. CHEN and J. A. DORMAN, "Investigations to Remove Domes from Plastic Shells by Polishing," *Fusion Sci. Technol.*, this issue.
10. K. C. CHEN, R. C. COOK, H. HUANG, S. A. LETTS, and A. NIKROO, "Fabrication of Graded Germanium-Doped CH Shells," *Fusion Sci. Technol.* **49**, 750 (2006).
11. H. HUANG, R. B. STEPHENS, S. A. EDDINGER, J. FUNTHER, A. NIKROO, K. C. CHEN, H. W. XU, "Nondestructive Quantitative Dopant Profiling Technique by Contact Radiography," *Fusion Sci. Technol.* **49**, 650 (2006).
12. G. E. SOMMARGREN, D. W. PHILLION, M. A. JOHNSON, N. Q. NGUYEN, A. BARTY, F. J. SNELL, D. R. DILLON, and L. S. BRADSHER, "100-Picometer Interferometry for EUVL," *Proc. SPIE* **4688**, 316 (2002).
13. J. L. KLINGMANN and G. E. SOMMARGREN, "Sub-Nanometer Interferometry and Precision Turning for Large Optical Fabrication," Lawrence Livermore National Laboratory Report UCRL-JC-134052 (1999).